Solution-Processed Fe3O4 Magnetic Nanoparticle Thin Film Aligned by an External Magnetostatic Field as a Hole Extraction Layer for Polymer Solar Cells

9 AUTHORS, INCLUDING:

Kai Wang
University of Akron
28 PUBLICATIONS **144** CITATIONS

SEE PROFILE

Chao Yi
University of Akron
21 PUBLICATIONS **99** CITATIONS

SEE PROFILE

Hao-Li Zhang
Lanzhou University
213 PUBLICATIONS **3,742** CITATIONS

SEE PROFILE

Alamgir Karim
University of Akron
307 PUBLICATIONS **6,951** CITATIONS

SEE PROFILE

Solution-Processed Fe_3O_4 Magnetic Nanoparticle Thin Film Aligned by an External Magnetostatic Field as a Hole Extraction Layer for Polymer Solar Cells

Kai Wang,[†] He Ren,[†] Chao Yi,[†] Chang Liu,[†] Hangxing Wang,[†,‡] Lin Huang,[§] Haoli Zhang,[‡] Alamgir Karim,[†] and Xiong Gong*,[†]

[†]College of Polymer Science and Polymer Engineering, The University of Akron, Akron, Ohio 44325, United States
[‡]State Key Laboratory of Applied Organic Chemistry, Lanzhou University, Lanzhou 730000, People's Republic of China
[§]Bruker Nano Surfaces Division, Santa Barbara, California 93117, United States

ABSTRACT: We report, for the first time, the effect of a solution-processed Fe_3O_4 magnetic nanoparticle (MNP) thin film and a Fe_3O_4 MNP thin film aligned by an external magnetostatic field, used as a hole extraction layer (HEL), respectively, in polymer solar cells (PSCs). The thin film of a Fe_3O_4 MNP shows a smoother surface, better transparency, and higher electrical conductivity than that of a poly(3,4-ethylenedioxythiophene):poly(styrenesulfonate) (PEDOT:PSS) thin layer. Moreover, the thin film of a Fe_3O_4 MNP aligned by an external magnetostatic field possesses an enhanced electrical conductivity and lower internal series resistance, thus leading to greater than 13% enhancement in the power conversion efficiency of PSCs than those using a PEDOT:PSS thin film. It was also found that PSCs incorporated with a Fe_3O_4 MNP shows better stability compared with those using PEDOT:PSS as an anode buffer layer.

These results demonstrated that utilization of a Fe_3O_4 MNP as a HEL in PSCs blazes a trail to achieve highly efficient and long-time-stable devices.

KEYWORDS: polymer solar cell, anode buffer layer, Fe_3O_4 magnetic nanoparticles, efficiency, stability, magnetostatic field
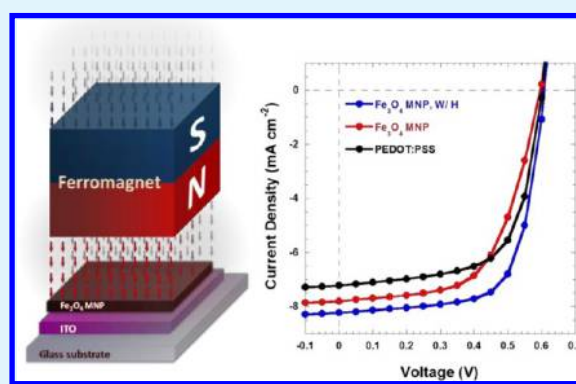
■ INTRODUCTION

In the past 2 decades, bulk heterojunction (BHJ) polymer solar cells (PSCs) have been attracting intense attention because of their advantages over traditional inorganic solar cells such as flexibility, low cost, light weight, large area, cleanliness, quietness, and processing simplicity.[1−4] Recent progresses in BHJ PSCs have shown a power conversion efficiency (PCE) of 12%,[5] which indicates that PSCs are strongly competitive with their inorganic counterparts. In PSCs, the BHJ composite is sandwiched between a poly(3,4-ethylenedioxythiophene):poly-(styrenesulfonate) (PEDOT:PSS)-coated indium−tin oxide (ITO) anode and a low-work-function cathode, e.g., calcium (Ca) or aluminum (Al); however, the acidic PEDOT:PSS etches ITO and causes device degradation during the operation of PSCs. One solution to circumvent the problem is to use p-type metal oxides such as MoO_3,[6−8] NiO,[9] and V_2O_5[10,11] as a hole extraction layer (HEL) to replace the PEDOT:PSS anode buffer layer. The PCEs of PSCs incorporating with a vacuum-deposited metal oxide as a HEL were comparable to those using a PEDOT:PSS anode buffer layer,[6−11] whereas the PCEs of PSCs incorporating a solution-processed metal oxide as a HEL were lower than those using a PEDOT:PSS anode buffer layer.[12,13] Therefore, looking for a suitable material as a HEL is

one ongoing research direction to enhance the performance of PSCs.[14]

Many materials have been utilized as a HEL in PSCs,[6−11] but the improvements in the PCEs are still not satisfying. Therefore, new approaches need to be investigated. Here, we report a facile method to enhance the efficiency and improve the stability of PSCs. Two types of Fe_3O_4 magnetic nanoparticle (MNP) thin films, pristine Fe_3O_4 and Fe_3O_4 MNPs aligned by an external magnetostatic field, were introduced as a HEL in PSCs. Significant enhancements in the efficiency and stability were observed from PSCs incorporated with Fe_3O_4 MNP thin films. To our best of knowledge, this is the first reported study on the effect of both a MNP thin film and MNP thin films aligned by an external magnetostatic field on the performance of PSCs.

■ EXPERIMENTAL SECTION

Materials. Poly(3-hexylthiophene-2,5-diyl) (P3HT) was purchased from Rieke Metals Inc. and used as received. [6,6]Phenyl-C61-butyric acid methyl ester ($PC_{61}BM$) was purchased from 1-Material Inc. and

Scheme 1. (a) Schematic Illustration of the Fabrication Procedure of a Solution-Processed Fe_3O_4 MNP, Followed by External Magnetostatic Field Alignment, as a HEL for PSCs and (b) the LUMO and HOMO Energy Levels of P3HT and PCBM and Work functions of PEDOT:PSS, Fe_3O_4, ITO, and Ca (Al)
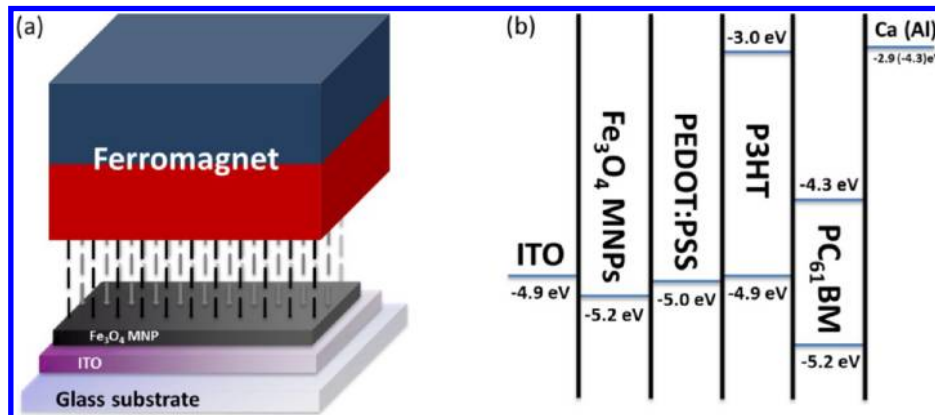
used as received. The oleic acid capped Fe_3O_4 MNP (5 mg mL^{-1} in toluene) was purchased from Sigma-Aldrich and used as received. The mean size of the oleic acid capped Fe_3O_4 MNP is about 5 nm. A square magnet (C750, $^3/_4$ in. cube, Licensed NdFeB) was purchased from Amazing Magnets Co.

Fe_3O_4 Thin Film Preparation. The ITO-coated glass substrates were first cleaned by the following procedures: wiping with detergent, rinsing with deionized water, and ultrasonicating in acetone and isopropanol sequentially for 30 min. Finally, the substrates were dried overnight in an oven. After ITO substrates were treated with UV ozone for 20 min under an ambient atmosphere, a thin film of a Fe_3O_4 MNP was cast from an oleic acid capped Fe_3O_4 MNP toluene solution on top of them. Subsequently, a thin film of a Fe_3O_4 MNP was thermally annealed at 300 °C for 45 min. As described in Scheme 1a, in order to fabricate a thin film of a Fe_3O_4 MNP aligned by an external magnetostatic field (represented by Fe_3O_4 MNP W/H), the Fe_3O_4 MNP thin film was aligned by an external vertical magnetostatic field with a magnetostatic field intensity of ca. 600 gauss with the film under thermal annealing. Such a magnetostatic field was generated by a magnet placed right above the ITO substrates (schematically shown in Scheme 1a). The thickness of the Fe_3O_4 MNP thin film is about 30 nm.

Thin Film Characterization. Tapping-mode atomic force microscopy (AFM) images were obtained by using a NanoScope NS3A system (Digital Instrument) to observe the surface morphologies and thicknesses of various thin films.

The transmission spectra of thin films of a Fe_3O_4 MNP (~30 nm thickness) and PEDOT:PSS (~30 nm) were measured using a HP 8453 spectrophotometer.

X-ray photoelectron spectroscopy (XPS) images were measured by a PHI 5000 Versa Probe II scanning XPS microprobe to identify the components of a solution-processed Fe_3O_4 MNP thin film after low-temperature annealing and/or external magnetostatic field alignment.

The surface electrical conductivities of Fe_3O_4 MNP thin films with and without external magnetostatic field alignment were conducted on a Bruker Dimension Icon system with a Peak Force Tapping Tunneling AFM (PFTUNA) module. The probe was a PFTUNA with a spring constant of ~0.5 N m^{-1} and 20 nm platinum/iridium coating on both the front and rear. The spring currents were measured with a bias voltage applied to the sample. The ramp rate of 0.4 Hz and the force set point of ~60 nN were used for both thin films.

PSC Fabrication and Characterization. In PSC devices, the BHJ composite is P3HT mixed with $PC_{61}BM$ (P3HT:$PC_{61}BM$ = 1:0.8 by weight). Approximately a 80-nm-thick P3HT:$PC_{61}BM$ thin film was cast from a P3HT:$PC_{61}BM$/dichlorobenzene (o-DCB) solution onto an ITO/Fe_3O_4 MNP substrate inside a glovebox within a nitrogen atmosphere. After that, 6-nm-thick Ca and then 100-nm-thick Al were sequentially vacuum-deposited on top of the BHJ composite with a

base pressure of 6×10^{-6} mbar through a shadow mask. The device area was 0.045 cm^2.

The current density–voltage (J–V) characteristics were obtained by using a Keithley model 2400 source measure unit. A Newport Air Mass 1.5 Global (AM1.5G) full-spectrum solar simulator was applied as the light source. The light intensity was 100 mW cm^{-2}, which was calibrated by utilizing a monosilicon detector (with a KG-5 visible color filter) of National Renewable Energy Laboratory to reduce the spectral mismatch. The incident photon-to-electron conversion efficiency (IPCE) spectra of PSCs were measured by a solar cell quantum efficiency measurement system (QEX10) from PV Measurements. The impedance spectra (IS) were obtained using a HP 4194A impedance/gain-phase analyzer, with an oscillating voltage of 10 mV and a frequency of 1 Hz to 1 MHz. PSCs were held at their respective open-circuit potentials, while the IS spectrum was being recorded.

■ RESULTS AND DISCUSSION

A Fe_3O_4 MNP was selected to serve as a HEL because these MNPs possess unique electrical, chemical, magnetic, optical, and anticorrosive properties.[15,16] Although various methods were used to fabricate a Fe_3O_4 MNP thin film, we present a simple approach for depositing a Fe_3O_4 MNP thin film from an oleic acid capped Fe_3O_4 MNP solution and then aligning the Fe_3O_4 MNP thin film by an external magnetostatic field. This approach allows us to use low-cost solution processing to fabricate a Fe_3O_4 MNP thin film as a HEL for BHJ PSCs. XPS was employed to investigate the major component of a solution-processed Fe_3O_4 MNP thin film. Figure 1 shows the XPS spectrum of a Fe_3O_4 MNP thin film. The Fe_3O_4 MNP thin film exhibited typical Fe 2p peaks of Fe_3O_4 at 723.4 and 710.3 eV, respectively. Also, typical Fe $2p_{1/2}$ and $2p_{3/2}$ lines are at 723.6 and 710.4 eV, respectively.[17] Thus, the major component of a Fe_3O_4 MNP thin film deposited from an oleic acid capped Fe_3O_4 MNP solution, whether followed by thermal annealing or external magnetostatic field alignment, is stoichiometrically confirmed to be Fe_3O_4.

The transmission spectra of thin films of Fe_3O_4 MNP and PEDOT:PSS coated on an ITO substrate are shown in Figure 2. Compared to that of a PEDOT:PSS thin film, better transmittance from 500 to 1100 nm are observed from a thin film of a Fe_3O_4 MNP, which indicates that a Fe_3O_4 MNP thin film is qualified to be a anode buffer layer, through which more visible light is able to transmit from the ITO/Fe_3O_4 MNP into a BHJ active layer without significant absorption losses.

AFM is used to study the thin-film morphology of Fe_3O_4 MNP and Fe_3O_4 MNP W/H. Figure 3 presents thin-film phase
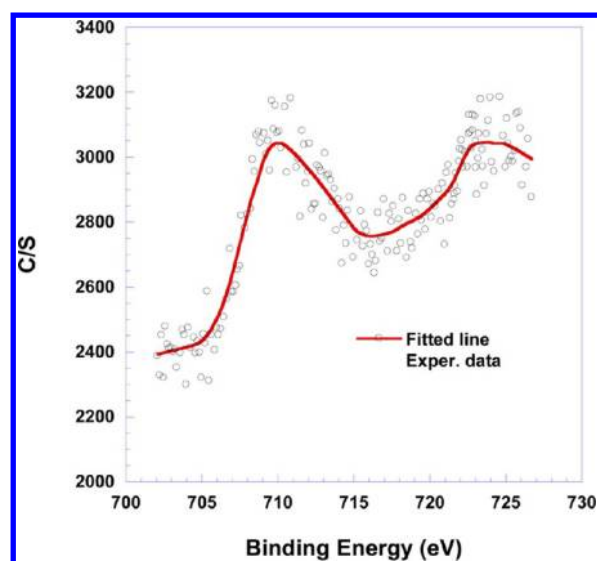
10326

dx.doi.org/10.1021/am4033179 | ACS Appl. Mater. Interfaces 2013, 5, 10325–10330

Figure 1. XPS Fe 2p core-level spectrum of the Fe_3O_4 MNP thin film.
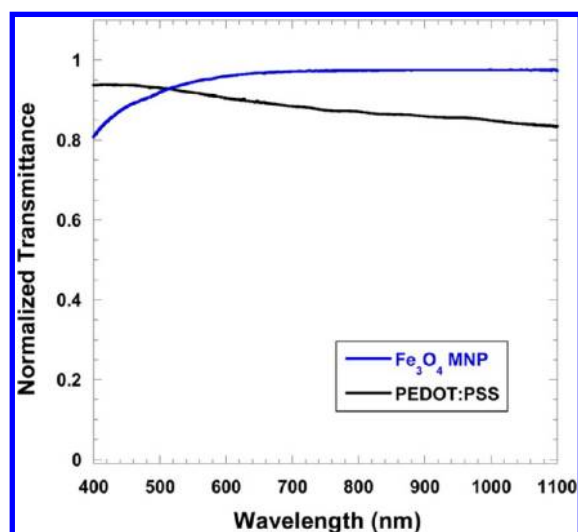
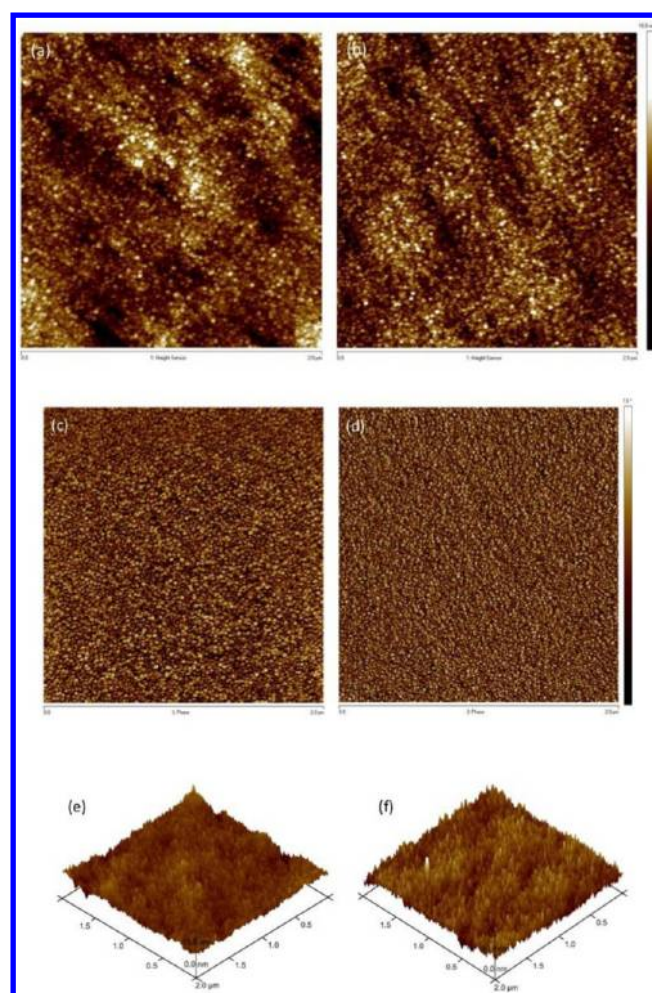**Figure 2.** Transmission spectra of PEDOT:PSS and Fe_3O_4 MNP thin films.

Figure 3. Tapping-mode AFM height images of Fe_3O_4 MNP thin films with (a) and without (b) external magnetostatic field alignment, phase images of Fe_3O_4 MNP thin films with (c) and without (d) external magnetostatic field alignment, and 3D height images of Fe_3O_4 MNP thin films with (e) and without (f) external magnetostatic field alignment.

images and height images of Fe_3O_4 MNPs with and without external magnetostatic field alignment. The nanoscale of Fe_3O_4 MNP W/H is larger than that of Fe_3O_4 MNP, indicating that the domain of a Fe_3O_4 MNP is enlarged after magnetic alignment. The root-mean-squared roughnesses of Fe_3O_4 MNP thin films with and without external magnetostatic field alignment are in the same scale region, but Fe_3O_4 MNP W/H is a little smoother than a Fe_3O_4 MNP from the 3D image. The smooth surface implies that a BHJ composite layer can be easily deposited on top of a Fe_3O_4 MNP W/H thin film and form a better contact with the BHJ active layer, thus leading to enhanced PCE. In addition, no sharp peak of ITO is observed from ITO/Fe_3O_4 MNP or ITO/Fe_3O_4 MNP W/H, indicating that the rough surface of the ITO substrate has been planarized well by the Fe_3O_4 layer.

The $J-V$ curves of BHJ PSCs under illumination are shown in Figure 4a. We calculated the series resistance (R_S) and shunt resistance (R_{SH}) from the slope of $J-V$ curves at 0 mA cm^{-2} and 0 V, respectively. The R_S and R_{SH} values from these three PSCs are summarized in Table 1. A low series resistance from PSCs with Fe_3O_4 MNP W/H is due to the small contact resistance and bulk resistance of the photoactive material, indicating that high currents will flow through the cell at low applied voltages. The large shunt resistance indicates that shorts or leakages of the photocurrent are minimal in the device. Under AM1.5G illumination with a light intensity of 100 mW cm^{-2}, an open-circuit voltage (V_{OC}) of 0.60 V, a short-circuit current density (J_{SC}) of 7.81 mA cm^{-2}, a fill factor (FF) of 54.5%, and a corresponding PCE of 2.55% were obtained from PSCs by using a Fe_3O_4 MNP as a HEL. At the same conditions, a V_{OC} of 0.61 V, a J_{SC} of 7.81 mA cm^{-2}, a FF of 53.7%, and a corresponding PCE of 2.70% were observed from PSCs by using Fe_3O_4 MNP W/H as a HEL. For PSCs with PEDOT:PSS as an anode buffer layer, a V_{OC} of 0.60 V, a J_{SC} of 7.22 mA cm^{-2}, a FF of 55.0%, and a corresponding PCE of 2.38% were observed. More than 80 devices were fabricated and characterized under the same conditions. The device performance parameters are summarized in Table 1. The deviation in the efficiencies of these devices is less than 5%. These results demonstrated that a Fe_3O_4 MNP thin film can be used as a HEL in PSCs, and PSCs using Fe_3O_4 MNP and Fe_3O_4 MNP W/H as a HEL, respectively, possessed higher performance
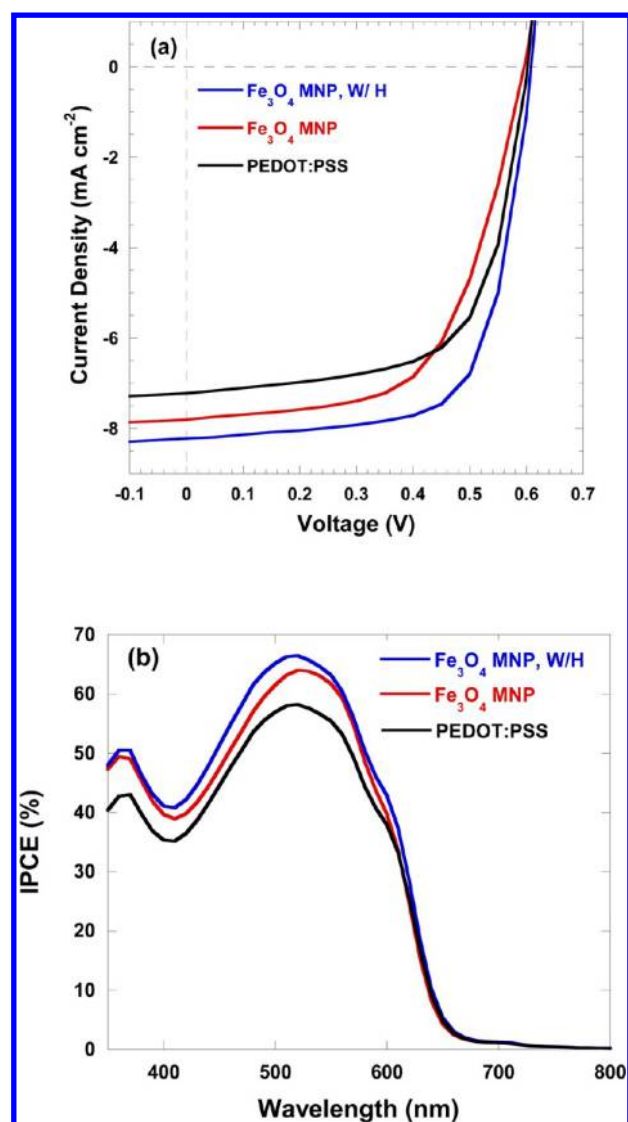
Figure 4. (a) Current density versus voltage (J–V) characteristics of PSCs measured under 100 mW cm^{-2} AM1.5 G illumination. (b) IPCE spectra of PSCs.

Table 1. Performance Parameters of PSCs

anode buffer layer	V_{OC} (V)	J_{SC} (mA cm^{-2})	R_{SH} (Ω cm^2)	R_S (Ω cm^2)	FF (%)	PCE (%)
PEDOT:PSS	0.60	7.22	1870	17.3	55.0	2.38
Fe$_3$O$_4$ MNP	0.60	7.81	965	16.0	54.5	2.55
Fe$_3$O$_4$ MNP W/H	0.61	8.25	1713	9.23	53.7	2.70

compared with those using PEDOT:PSS as an anode buffer layer.

The PSCs were further characterized by IPCE spectroscopy. As shown in Figure 4c, the integrated J_{SC} from IPCE are 7.20, 7.77, and 8.23 mA cm^{-2} for PSCs incorporated with PEDOT:PSS, Fe$_3$O$_4$ MNP, and Fe$_3$O$_4$ MNP W/H thin films, respectively. All calculated J_{SC} values are consistent with those obtained from the J–V characteristics.

In order to analyze enhanced PCEs of PSCs, the internal series resistance (R_S) of PSCs incorporated with Fe$_3$O$_4$ MNP by IS was investigated and compared with those from PSCs using PEDOT:PSS as a buffer layer. R_S of PSCs consists of

sheet resistance (R_{SH}; contact resistance between the BHJ composite and adjacent electrodes, resistance associated with probe lines and interconnections, etc.) and charge-transport resistance (R_{CT}, bulk resistivity of semiconducting materials).[18] The IS analysis enabled us to monitor the specific electrical properties of the interfaces that cannot be determined by direct-current measurements.[19] The only difference of PSCs with various HELs in our investigation is in R_{SH}. The Nyquist plots of PSCs were measured at an applied voltage of 0.6 V under AM1.5G illumination with a light intensity of 100 mW cm^{-2} and are shown in Figure 5a. From the plots, the resistance
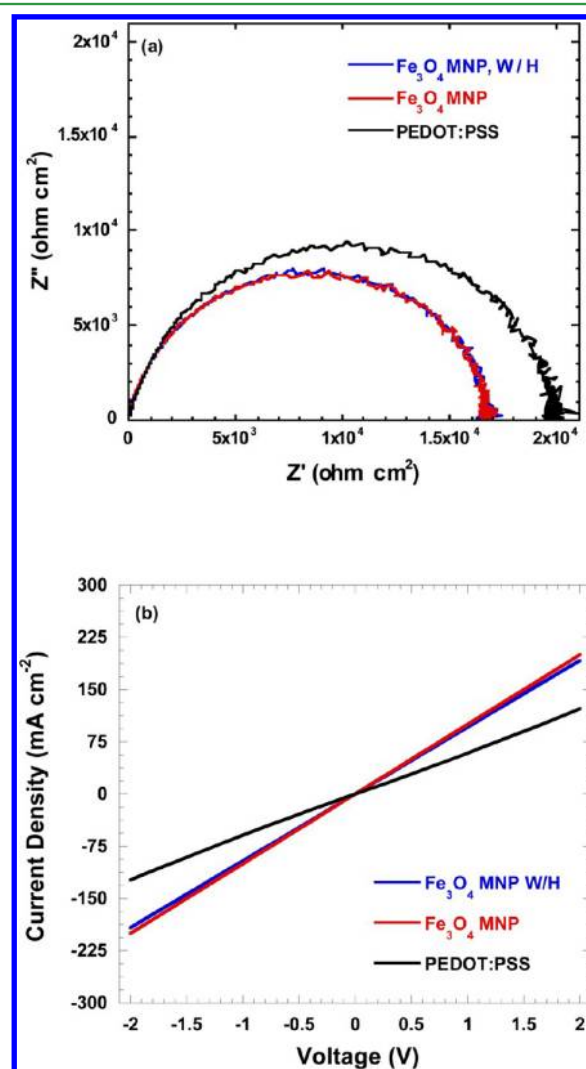

Figure 5. (a) Nyquist plots measured at $V = V_{OC}$. (b) J–V characteristics of ITO/thin films/Al devices, where thin films are PEDOT:PSS, Fe$_3$O$_4$ MNP, and Fe$_3$O$_4$ MNP W/H, respectively.

of PSCs using PEDOT:PSS as an anode buffer layer is ca. 19.9 Ω cm^2 and ca. 16.8 Ω cm^2 for PSCs using Fe$_3$O$_4$ MNP as a HEL. A resistance of 16.8 Ω cm^2 is observed from PSCs using Fe$_3$O$_4$ MNP W/H as a HEL. These results demonstrated that the charge-transfer resistances of PSCs using Fe$_3$O$_4$ MNP as a HEL are reduced compared with that using PEDOT:PSS as an anode buffer layer. Thus, a high performance is anticipated from PSCs incorporating a Fe$_3$O$_4$ MNP.

We further investigated the electrical conductivity of Fe$_3$O$_4$ MNP thin films by evaluating the J–V curves observed from a
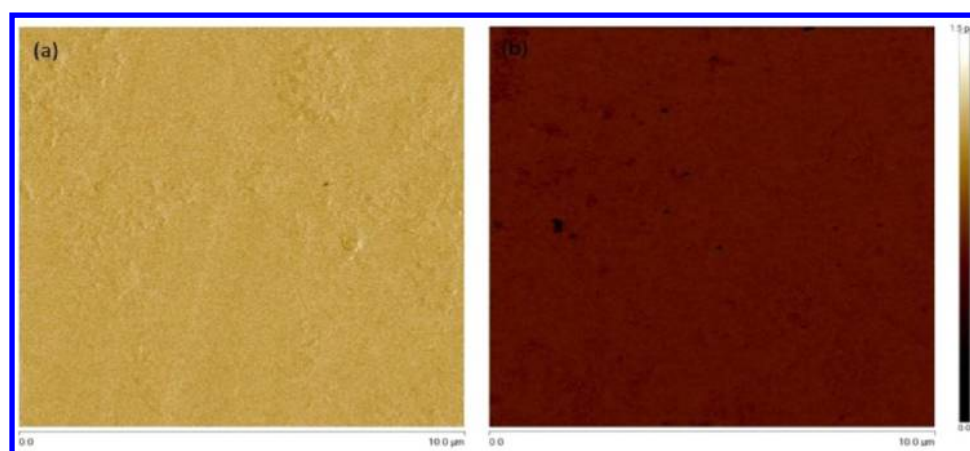
Figure 6. Peak currents of Fe_3O_4 MNP thin films with (a) and without (b) external magnetostatic field alignment.

sandwiched device with a structure of ITO/thin film/Al.[20,21] Figure 5b displays the $J-V$ curves of ITO/thin film/Al devices, where thin films are a PEDOT:PSS layer, a Fe_3O_4 MNP layer, and a Fe_3O_4 MNP W/H layer, respectively. The thicknesses of these layers were controlled to be identical with the value of 30 ± 1.4 nm. At the same applied voltages, both Fe_3O_4 MNP and Fe_3O_4 MNP W/H possess similar current densities, while the PEDOT:PSS thin film possesses the lowest current densities among these three thin films. For example, at 2 V, the current density of Fe_3O_4 MNP thin films with and without external magnetostatic field alignment is ca. 200 mA cm^{-2}, which is larger than ca.122 mA cm^{-2} observed from that of the PEDOT:PSS thin film. Moreover, $J-V$ curves of Fe_3O_4 MNP and Fe_3O_4 MNP W/H are linear and symmetric, which is similar to that of the PEDOT:PSS thin film, indicating that an ohmic contact between the ITO anode and Fe_3O_4 MNP thin film is formed.[22] This observation is consistent with the band alignment shown in Scheme 1b (the Fermi level of Fe_3O_4 is cited from ref 34). The ohmic contact formed between the ITO anode and Fe_3O_4 MNP HEL implies that there is no barrier for Fe_3O_4 MNP HEL to extract and transport separated holes from the BHJ composite.

In order to further understand the underlying of enhanced PCE, the surface electrical conductivities of Fe_3O_4 MNP and Fe_3O_4 MNP W/H were conducted by PFTUNA measurement. The peak currents are shown in Figure 6. At the same condition (zoom size), Fe_3O_4 MNP W/H shows a surface electrical conductivity of 1.15 pA, which is nearly twice as high as that of Fe_3O_4 MNP (0.67 pA). These results indicated that external magnetostatic fields probably change the molecular alignment within Fe_3O_4 MNP and alter the surface electrical conductivity of Fe_3O_4 MNP.

Studies have shown that dipoles would be generated when MNP was aligned by an external magnetostatic field. In particular, an external magnetostatic field exerts a torque on MNP, thus producing magnetic dipole moments, which drives MNP to polarize within an external magnetostatic field.[23-25] In a Fe_3O_4 MNP thin film, the "head-to-tail" structure of a Fe_3O_4 MNP is formed to minimize the systematic energy,[23] while if an external magnetostatic field is vertically positioned to Fe_3O_4 MNP, Fe_3O_4 MNP will form a separated isotropic structure because of parallel moment repulsion, which leads to changes of the film morphology and enhances the surface electrical conductivity of a Fe_3O_4 MNP thin film.[26-29] In addition, an extra dipole will enhance charge separation and transportation

within a HEL.[30] The dipoles of a Fe_3O_4 MNP are random in all directions without an external magnetostatic field alignment. After external magnetostatic field alignment, a Fe_3O_4 MNP is rearranged in a certain order by the mechanism of magnetic dipolar interaction. Spontaneously, the dipoles of a Fe_3O_4 MNP were parallel in the presence of a vertically applied magnetostatic field. This will drive a Fe_3O_4 MNP thin film to generate an electric field. This electric field, with the electric field generated by two electrodes because of different work functions, would drive more separated charge carriers to transport to the corresponding electrodes compared with those using a Fe_3O_4 MNP HEL without magnetostatic field alignment.[31-33] Therefore, PSCs using Fe_3O_4 MNP W/H as a HEL possess higher performance compared with those using a Fe_3O_4 MNP as a HEL.

We also studied the stability of PSCs. We tested the devices every 12 h. The results of self-stability of PSCs are shown in Figure 7. By using a Fe_3O_4 MNP to replace PEDOT:PSS, the stabilities of PSCs are significantly enhanced. For PSCs with a Fe_3O_4 MNP as a HEL, PCEs remained at approximately 95% of the original value for 72 h, while PCEs of PSCs with PEDOT:PSS as an anode buffer layer degraded evidently by 10%. The half-life of PSCs with a Fe_3O_4 MNP as a HEL is nearly 600 h, but that of PSCs using PEDOT:PSS is only about
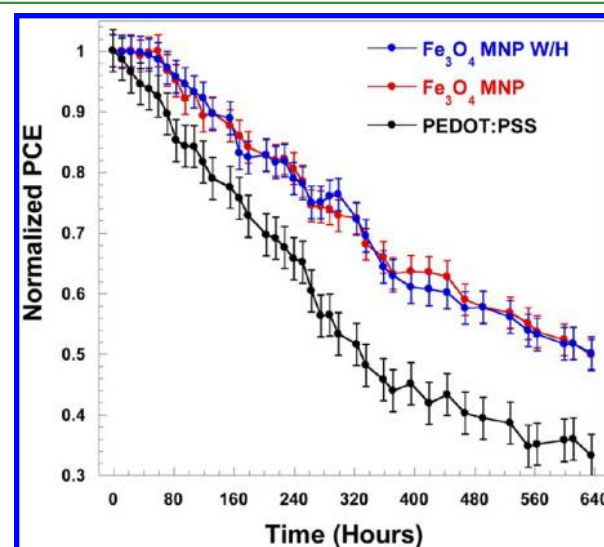

Figure 7. Shelf-stability of PSCs.

300 h. Therefore, utilization of a Fe_3O_4 MNP as a HEL in BHJ PSCs can significantly improve the air stability of PSCs.

■ CONCLUSIONS

Efficient and stable BHJ PSCs by using a thin layer of a Fe_3O_4 MNP as a HEL were fabricated. Efficiencies observed from PSCs using Fe_3O_4 MNP as a HEL show higher PCEs than those using PEDOT:PSS as an anode buffer layer and the stability of PSCs is significantly enhanced. We further found that PSCs using a thin layer of Fe_3O_4 MNP, followed with external magnetostatic field alignment exhibiting both enhanced efficiency and dramatically enhanced stability compared with those using PEDOT:PSS as an anode buffer layer. Our finding demonstrated that utilization of Fe_3O_4 MNP as a HEL in PSCs blazes a trail to achieve highly efficient and long-time-stable PSCs.

■ AUTHOR INFORMATION

Corresponding Author
*E-mail: xgong@uakron.edu. Fax: (330) 972-3406.

Notes
The authors declare no competing financial interest.

■ REFERENCES

(1) Günes, S.; Neugebauer, H.; Sariciftci, N. S. *Chem. Rev.* **2007**, *107*, 1324−1338.
(2) Clemens, W.; Fix, W.; Ficker, J.; Knobloch, A.; Ullmann, A. *J. Mater. Res.* **2011**, *19*, 1963−1973.
(3) Brabec, C. J.; Sariciftci, N. S.; Hummelen, J. C. *Adv. Funct. Mater.* **2001**, *11*, 15−26.
(4) Günes, S.; Neugebauer, H.; Sariciftci, N. S. *Chem. Rev.* **2007**, *2*, 145−154.
(5) *Heliatek.* Available at HYPERLINK, http://www.heliatek.com.
(6) Kim, D. Y.; Subbiah, J.; Sarasqueta, G.; So, F.; Ding, H.; Gao, Y. *Appl. Phys. Lett.* **2009**, *95*, 093304.
(7) Subbiah, J.; Kim, D. Y.; Hartel, M.; So, F. *Appl. Phys. Lett.* **2010**, *96*, 063303.
(8) Tao, C.; Ruan, S.; Xie, G.; Kong, X.; Shen, L.; Meng, F.; Liu, C.; Zhang, X.; Dong, W.; Chen, W. *Appl. Phys. Lett.* **2009**, *94*, 043311.
(9) Steirer, K. X.; Chesin, J. P.; Widjonarko, N. E.; Berry, J. J.; Miedaner, A.; Ginley, D. S.; Olson, D. C. *Org. Electron.* **2010**, *11*, 1414−1418.
(10) Chen, L.-M.; Xu, Z.; Hong, Z.; Yang, Y. *J. Mater. Chem.* **2010**, *20*, 2575−2598.
(11) Li, G.; Chu, C.-W.; Shrotriya, V.; Huang, J.; Yang, Y. *Appl. Phys. Lett.* **2006**, *88*, 253503.
(12) Lee, Y.-J.; Yi, J.; Gao, G. F.; Koerner, H.; Park, K.; Wang, J.; Luo, K.; Vaia, R. A.; Hsu, J. W. P. *Adv. Eng. Mater.* **2012**, *2*, 1193−1197.
(13) Stubhan, T.; Ameri, T.; Salinas, M.; Krantz, J.; Machui, F.; Halik, M.; Brabec, C. J. *Appl. Phys. Lett.* **2011**, *98*, 253308.
(14) Hatton, R. A.; Blanchard, N. P.; Tan, L. W.; Latini, G.; Cacialli, F.; Silva, S. R. P. *Org. Electron.* **2009**, *10*, 388−395.
(15) Gupta, A. K.; Gupta, M. *Biomaterials* **2005**, *26*, 3995−4021.
(16) Laurent, S.; Forge, D.; Port, M.; Roch, A.; Robic, C.; Vander Elst, L.; Muller, R. N. *Chem. Rev.* **2008**, *108*, 2064−110.
(17) Joong, K.; Won, D.; Kyung, S.; Jung, K. *Thin Solid Films* **2000**, *360*, 118−121.
(18) Deibel, C.; Dyakonov, V. *Rep. Prog. Phys.* **2010**, *73*, 096401.
(19) Jo, S. J.; Kim, C. S.; Kim, J. B.; Ryu, S. Y.; Noh, J. H.; Baik, H. K.; Kim, Y. S.; Lee, S.-J. *J. Appl. Phys.* **2008**, *103*, 114502.
(20) Liang, Y.; Xu, Z.; Xia, J.; Tsai, S.-T.; Wu, Y.; Li, G.; Ray, C.; Yu, L. *Adv. Mater.* **2010**, *22*, E135−E138.
(21) Chen, L.-M.; Hong, Z.; Li, G.; Yang, Y. *Adv. Mater.* **2009**, *21*, 1434−1449.
(22) MacDonald, G. A.; Veneman, P. A.; Placencia, D.; Armstrong, N. R. *ACS Nano* **2012**, *6*, 9623−9636.
(23) Zhang, W.; Sun, J.; Bai, T.; Wang, C.; Zhuang, K.; Zhang, Y.; Gu, N. *ChemPhysChem* **2010**, *11*, 1867−1870.
(24) Mørup, S.; Hansen, M. F.; Frandsen, C. *Beilstein J. Nanotechnol.* **2010**, *1*, 182−190.
(25) Hansen, M. F.; Mørup, S. *J. Magn. Magn. Mater.* **1998**, *184*, 262−274.
(26) Svozil, K. *Phys. Rev. Lett.* **1985**, *54*, 742−744.
(27) Ji, J.-Y.; Held, E. D.; Sovinec, C. R. *Phys. Plasmas* **2009**, *16*, 022312.
(28) Atwood, D.; Aeppli, A.; Soni, A. *Phys. Rev. Lett.* **1992**, *69*, 2754−2757.
(29) Love, J. C.; Urbach, A. R.; Prentiss, M. G.; Whitesides, G. M. *J. Am. Chem. Soc.* **2003**, *125*, 12696−12697.
(30) Nalwa, K. S.; Carr, J. A.; Mahadevapuram, R. C.; Kodali, H. K.; Bose, S.; Chen, Y.; Petrich, J. W.; Ganapathysubramanian, B.; Chaudhary, S. *Energy Environ. Sci.* **2012**, *5*, 7042−7049.
(31) Zhang, W.; Sun, J.; Bai, T.; Wang, C.; Zhuang, K.; Zhang, Y.; Gu, N. *ChemPhysChem* **2010**, *11*, 1867−1870.
(32) Hwang, J. G.; Zahn, M.; O'Sullivan, F. M.; Pettersson, L. A. A.; Hjortstam, O.; Liu, R. *J. Appl. Phys.* **2010**, *107*, 014310.
(33) Shvydka, D.; Karpov, V. G. *Appl. Phys. Lett.* **2008**, *92*, 053507.
(34) Pratt, A.; Dunne, L.; Sun, X.; Kurahashi, M.; Yamauchi, Y. *J. Appl. Phys.* **2012**, *111*, 07C114.